The Thesis Committee for Kade J. Kearney
Certifies that this is the approved version of the following Thesis:

Assessment of a Cryogenic Coring Method to Preserve Depth-Discrete Distributions of Trichloroethylene and Volatile Reaction Products in a Low-Permeability Aquitard

APPROVED BY
SUPERVISING COMMITTEE:

Charles Werth, Supervisor

Manish Kumar

Assessment of a Cryogenic Coring Method to Preserve Depth-Discrete Distributions of Trichloroethylene and Volatile Reaction Products in a Low-Permeability Aquitard

by

Kade J. Kearney

Thesis

Presented to the Faculty of the Graduate School of

The University of Texas at Austin

in Partial Fulfillment

of the Requirements

for the Degree of

Master of Science in Engineering

The University of Texas at Austin

August 2022

Acknowledgements

The author would like to thank their advisor and mentor, Dr. Charles Werth, in supporting this work, and members of the Werth Research Group: Timothy Blount, Rosemary Arvizu, Lang Zhou, and Emma Palmer. They would also like to thank their family and friends for their continual support for and curiosity in their work.

Abstract

Assessment of a Cryogenic Coring Method to Preserve Depth-Discrete Distributions of Trichloroethylene and Volatile Reaction Products in a Low-Permeability Aquitard

Kade J. Kearney, M.S.E

The University of Texas at Austin, 2022

Supervisor: Charles J. Werth

Back diffusion of trichloroethylene (TCE) from low permeability zones (LPZs), such as clay aquitards, presents a challenge in attainment of site cleanup goals. There is not a clear understanding of the extent by which naturally occurring reactions can attenuate TCE and its daughter products within the LPZs. In this study, a soil coring method that freezes the soil in-situ (a.k.a., cryogenic coring) was utilized to measure depth-discrete distributions of TCE and its volatile reaction products through a TCE-impacted silty clay aquitard. The results were compared with those from adjacent soil cores taken using a conventional coring approach, and found the two coring methods recovered statistically equivalent concentrations of select volatiles across most depths. Biotic reductive dechlorination was found to be the dominant TCE reaction pathway at the site, and concentrations of TCE, cis-1,2-dichloroethylene (DCE), vinyl chloride (VC), ethane, and methane were all compared between the two coring methods. Benefits of the cryogenic coring were better recovery of dispersed sand layers and more variable concentration profiles for TCE, DCE, and VC.

Table of Contents

List of Tables

List of Figures

1.0 Introduction

1.1 BACKGROUND

Back diffusion of trichloroethylene (TCE) and its daughter products from low permeability zones (LPZs) such as clay lenses represents a long-term source of groundwater contamination. Plume concentrations can exceed site clean-up goals for decades, and it is unclear how both biotic and abiotic transformation reactions within LPZs can reduce mass transfer rates of back diffusion to adjacent high permeability zones (HPZs) and hasten site closure (Berns et al., 2019; Parker et al., 2008). The volatile reaction products of biotic and abiotic TCE reactions, especially the reduced gases associated with abiotic reduction, are difficult to measure in-situ due to losses associated with conventional coring and preservation methods. A relatively new cryogenic coring method that freezes the soil core in place, prior to extraction, has emerged as an alternative to preserve in-situ conditions and improve detection of these chemicals. This is important because subsurface depth profiles of TCE and volatile reaction products can be used to enhance conceptual site models, identify relevant reaction pathways, and possibly estimate natural attenuation rates within LPZs.

Proposed biotic and abiotic reaction pathways for TCE under anaerobic conditions are illustrated in Figure 1 (Arnold & Roberts, 2000; Lee & Batchelor, 2004; Schaefer et al., 2017a, 2021; Vogel & McCarty, 1985). For biotic transformation to take place, a suitable electron donor and dechlorinating bacteria (e.g. *Dehalococcoides* genus) must be present to reduce TCE through cis-1,2-dichloroethene (DCE) and vinyl chloride (VC), all the way to ethene. However, site limitations often cause the reaction to stall, and DCE and/or VC to accumulate. Abiotic transformation reactions typically occur in the presence of reactive ferrous minerals (e.g. mackinawite (Fe-S_{am}), green rusts, and ferrous iron-rich

clays, (Ferrey et al., 2004; Hayes, 1999; He et al., 2010; Jeong & Hayes, 2007; Lee & Batchelor, 2002, 2004; Schaefer et al., 2017b), and most abiotically converted TCE mass has been recovered as acetylene (C. Butler & F. Hayes, 1999). However, acetylene can be transformed to ethane or ethene via biotic (Koene-Cottaar & Schraa, 2006) and abiotic (Arnold & Roberts, 2000) reaction pathways. Further transformation products such as propane and butane, among other volatile compounds (Fig. 1), have been detected during abiotic TCE reduction experiments (Schaefer et al., 2017a). Thus, there is great interest in preserving in-situ conditions for sampling these volatile TCE reaction products to probe active reaction pathways for TCE in LPZs.

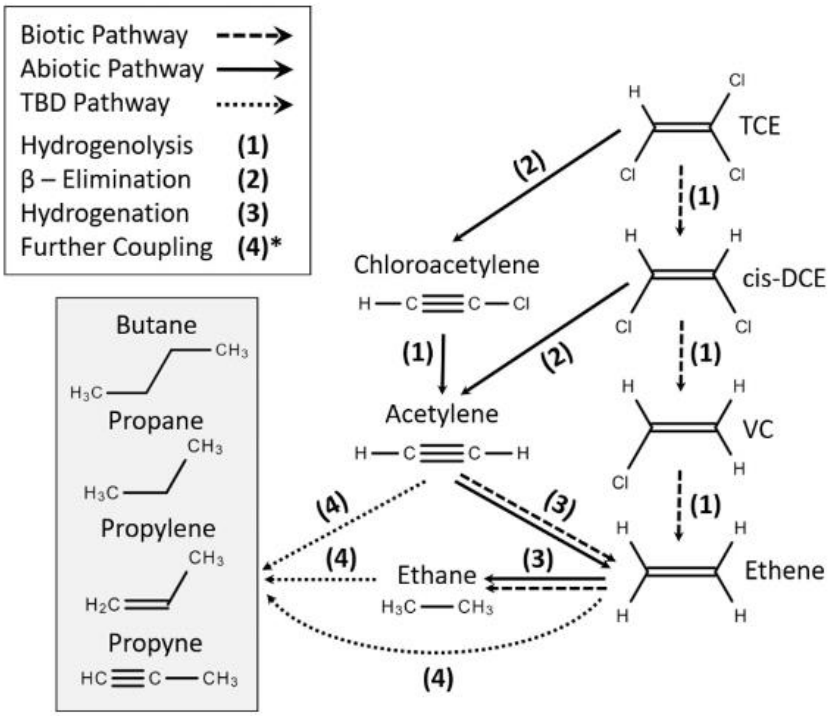

Figure 1: Biotic and abiotic reduction pathways of trichloroethylene (TCE). Further coupling products have been measured alongside TCE reduction experiments and the pathways are not well understood (Schaefer et al., 2013).

Cryogenic coring has been proposed as an alternate sample collection technique to preserve in-situ conditions. This coring method employs a conventional hollow-stem auger technique, attached to a cooling system that circulates liquid nitrogen through a dual-wall to freeze the soil in place. Benefits from this coring technique over conventional methods are improved recovery of cohesionless sediment, mitigation of flowing sands during sampling, greater preservation of biologic gene expressions, prevention of pore water drainage, and enhanced preservation of redox-active soil characteristics (Kiaalhosseini et al., 2016; Kocur et al., 2020; McCall et al., 2014; Richards et al., 2019). Cryogenic coring may also better preserve volatile organic compound (VOC) concentrations by protecting the soil core from sudden exposure to oxygen or elevated temperatures, and mitigating diffusion or reaction of compounds, as a result of bringing the core to surface frozen.

1.2 OBJECTIVES

The primary objectives of this work are to (1) assess if cryogenic coring better preserves TCE and its volatile reaction products versus a conventional coring approach applied at the same time and location, and (2) to determine if abiotic reactions are contributing to TCE attenuation at an impacted field site. To address these objectives, both cryogenic and conventional cores were taken side-by-side at a TCE-impacted groundwater site located on a Department of Defense (DOD) facility, processed, and then sampled for TCE and its volatile reaction products. Geochemical parameters were additionally measured to help interpret possible TCE transformation pathways. To date, no study has completed a robust comparison of volatiles recovery between cryogenic and conventional coring. Additionally, detection of acetylene in-situ has proven difficult and could result in underestimates of abiotic TCE natural attenuation rates if it is lost in the sampling process.

2.0 Materials & Methods

2.1 Site Description

Lake City Army Ammunition Plant (LCAAP) is a DOD ammunition manufacturing facility located in Independence, Missouri. The investigation area at LCAAP (Figure 2) was a disposal site for buried munitions, solvents, and other various wastes between 1960 and 1975. Release of TCE to the groundwater was first documented in 1982 and a Record of Decision (RoD) was finalized in 1998 to address the primary contaminants of concern (CoCs), TCE and its associated biodegradation products, cis-1,2-DCE and VC, in the groundwater (Environmental Protection Agency, 1998). Active remedial efforts at this site include gravity-fed injections of an emulsified vegetable oil at various injection wells (Fig. 2) downgradient of the source area to stimulate biodegradation of the chlorinated solvents. There have not been direct actions to remove the source of contamination at the southeast corner of the site, and DNAPL was identified in monitoring well MW-103 during this investigation (which coincides with the location of DNAPL in Fig. 2).

Site lithology is dominated by an unconsolidated silty clay overburden with pockets of trace gravel and sand that extends to approximately 6 meters in depth (Keller et al., 2003). Below the silty clay is a weathered bedrock layer for another 6-10 meters in depth, before a competent bedrock layer is expected to be present. Dispersed throughout the site are shallow paleochannel sand layers that are thought to be connected with Abshier Creek, bordering the north and east portions of the site. The depth to groundwater during investigation was 2.75 m-bgs, but ranges between 1.5-4.0 m-bgs at the site, and flows generally to the northwest with an average hydraulic gradient of 0.025 ft/ft (Keller et al., 2003).

The presence of cis-1,2-dichloroethylene (DCE) and vinyl chloride (VC) in the groundwater is indicative of biotic TCE reduction occurring at the site. At MW-103, where the DNAPL source zone is indicated in Fig. 2, the historical ratio of TCE to DCE obtained from measurement taken from 2012 to 2015 is 1.28±0.2, indicating TCE and DCE are both present in the source area, and that DCE on-site is sourced from disposed solvent and/or biotic reduction of TCE that occurred prior to source zone measurements. Although there is no direct evidence of abiotic TCE reactions occurring at the site prior to this work, the reducing environment required for biotic TCE reduction would be favorable to iron-reduction and thus potential formation of reactive iron minerals capable of abiotic TCE reduction (Butler & Hayes, 2001; Y. T. He et al., 2015).

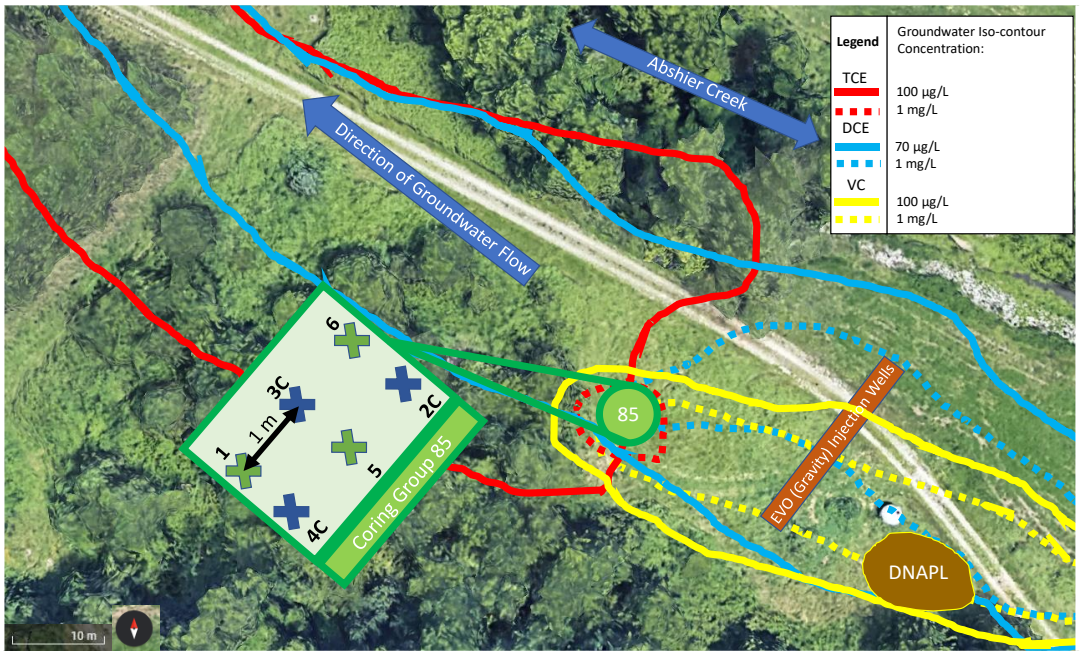

Figure 2: Site layout of Area 17D at LCAAP. Monitoring well MW-103 is located within the DNAPL source area. Overlapping plumes of TCE, 1,2-cis-DCE, and VC are all detected at the site, with the most concentrated portion of the TCE plume being at Coring Group 85. Groundwater flow is generally to the northwest.

2.2 Conventional and Cryogenic Soil Core Collection

Soil samples were collected from the field site in August 2021 using a CME-75 drill rig with a hollow stem auger fitted with a dual wall cooling cylinder for *in-situ* freezing of the soil core using liquid nitrogen, as previously described (Kiaalhosseini et al., 2016). A total of six cores were collected, three conventionally (hollow stem auger without freezing) and another three using the cryogenic freezing, at the coring location denoted as Coring Group 85 (CG85) in Figure 2. CG85 is approximately 50 meters downgradient of the DNAPL source zone, along the direction of groundwater flow. Core samples were taken from 2.0-7.5 m-bgs at CG85 with a sampling interval of 0.75 meters. Recovery beyond the full 0.75 meters was not used in the analysis as it was not contained within the PVC core liner. The borings at each location are spaced one meter apart from one another and their orientation is depicted in Figure 2, perpendicular to the direction of groundwater flow. All soils cores were measured for soil recovery, immediately placed in a cooler with dry ice, shipped to the University of Texas Austin, and stored at -20°C until analysis.

2.3 Volatiles Analysis

The frozen soil core samples were processed using a DeWalt chop saw, cutting out 2.5 cm intervals that were crushed frozen and quickly funneled into pre-weighed, 30 mL borosilicate glass serum bottles. The bottles were crimp sealed with Teflon-lined butyl stoppers and the soil was allowed to thaw for at least 12 hours at room temperature (23°C). Next, the headspace of the bottles was analyzed by injecting 200 µL using a gas-tight, glass syringe, into an Agilent 6890 gas chromatograph with a flame-ionization detector (GC-FID), using a GS-Q column (30m x 320 µm x 0.2 µm). Standards for reduced gasses were created using a 15 ppm_v (in N_2) gas tank of ethene, ethane, methane, propene, propane, and methyl acetylene. Vinyl chloride standards were made using a 1000 ppm_v (in N_2) gas tank.

TCE and DCE standards were created by diluting a methanol stock solution in 100 mL NPW with 60 mL headspace, and concentrations calculated using their respective dimensionless Henry's constant values ($H_{cc,i}$) for headspace partitioning. Five-point standards were used for all analytes and are presented in the SI. Headspace concentrations were used to calculate total analyte masses per mass of dry soil via mass balance, using measured water saturations, dry soil masses (m_{soil}), and an equilibrium distribution coefficient (Kd) approximated from the measured fraction of organic carbon (foc), literature values of the octanol-water partition coefficient (Kow), and Karickhoff's relationship between these parameters (Karickhoff et al., 1979). Equations, assumptions, and constants used are detailed in the SI. A total of 190 samples were completed for volatiles analysis across the six cores, with samples taken at intervals ranging from 7.5-15 cm.

2.4 GEOCHEMICAL ANALYSIS

All geochemical analyses were conducted using frozen quarters of 2.5 cm soil core sections collected at different depths. Ferrous mineral content was determined by McCampbell Analytical, Inc. using the 1,10-phenanthroline method (SM3500-Fe B4c) (Amonette & Charles Templeton, 1998). Total iron content was determined using inductively coupled plasma – optical emission spectroscopy (ICP-OES), following a sequential nitric acid and hydrogen peroxide digestion over three days, with 10-hr heating (150°C) periods in between (8 mL acid, 2 mL H_2O_2 per gram of soil). Chemical oxygen demand (COD) was measured using TNT 821 Hach Kits. Soil water mass and bulk density was calculated based upon mass comparisons between 24-hr heating cycles at 105°C (see SI). The soil's organic content was determined by mass comparisons after heating the soil

at 360°C; calculation of f_{oc} is provided in the SI. They were obtained from three different soil samples obtained at 3.5 m-bgs, 5.5 m-bgs, and 7.0 m-bgs.

3.0 Results & Discussion

3.1 More Sand Recovery is Obtained by Cryogenic versus Conventional Coring

Comparison of soil recovery in the CG85 cores is illustrated in Figure 3. The lithology is consistent with that expected from previous investigations; a silty clay dominates the shallow subsurface to 5.0 – 6.0 m-bgs, with some trace gravel and sands above 4.0 m-bgs. The soil transitions to a denser clay at about 6.0 m-bgs, followed by a clayey bottom that will transition to the underlying weathered shale formation. Distinct sand lenses were recovered only in cryogenic cores CG85-4C and CG85-2C at depths of 4.6 – 4.9 (4C only), 5.9 – 6.3, and 6.7 – 7.3 m-bgs. Sand lenses were never recovered in conventional cores, which had significantly less soil recovery over the depths that sand was preserved in the cryogenic cores. It is unlikely a coincidence that the conventional cores had less recovery at all three of the known sand layer depths. The cryogenic coring method was developed to directly address the difficulty of recovering saturated non-cohesive sediments, and it appears it was effective in preserving subsurface lithology (Kiaalhosseini et al., 2016).

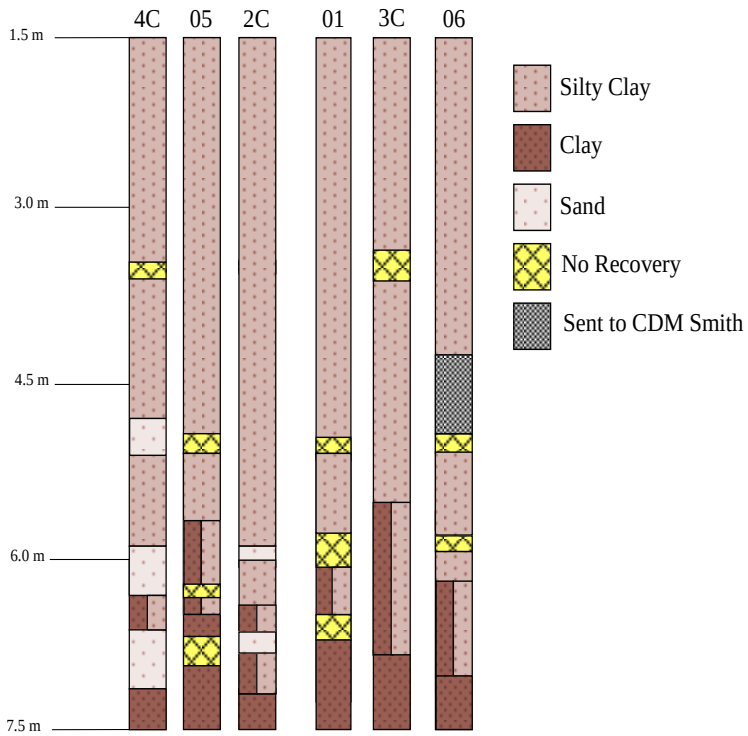

Figure 3: Lithology profiles from all six cores in CG85. Layout of figure is related to orientation of borings in the field (3x2), with 4C/05/2C one-meter upgradient of 01/3C/06. Loss of soil during sampling is indicated by the yellow intervals. One 0.75-meter section of 85-06 was not analyzed for volatiles and was instead sent to CDM Smith.

Also notable are the differences in sand recovery between adjacent cryogenic cores at CG85. Sand is recovered at three depth intervals in CG85-4C, the same two lower intervals in CG85-2C but in lower amounts, and not at all in CE85-3C despite full core recovery at depths where sand was recovered in the other cores. This indicates that the paleochannel sand lenses are heterogeneously dispersed across the site, both horizontally and vertically. These sand layers are likely contributing to plume persistence via back diffusion of TCE from the adjacent silty clay layers, and knowledge of their exact depths is critical for development of accurate site conceptual models (Chapman & Parker, 2005).

The TCE plume on-site is over 2,000' in length, which, even over decades, would not be possible by only diffusion through the silty clay portions of the subsurface.

Curiously, the recovered sand was always hollow, meaning that core sections with sand had an ice center surrounded by a layer of frozen sand that was approximately 1-2.5 cm thick. During cryogenic coring, liquid nitrogen circulated just outside the PVC liner. The liquid nitrogen froze sand adjacent to the PVC liner, but apparently not sand in the core center. This unfrozen sand was lost during core retrieval, and likely backfilled by adjacent groundwater that subsequently froze. Therefore, analysis of sand layers is influenced by analytes in adjacent groundwater, not just in soil.

3.2 Biotic, But Not Abiotic, Reductive Pathways Are Indicated by VOC Trends in Soil Cores

Representative vertical profiles of total VOCs (i.e., both CVOCs and reduced gases) per dry soil mass from cryogenic core CG85-4C are presented in Figure 4 on two different concentration scales, along with core lithology and discrete measurements of sediment-associated ferrous (Fe(II)) and total iron. Vertical profiles of total VOCs for the remaining cores at CG85 are presented in Figure 5. For CG85-4C (Figure 4), TCE and DCE are mainly present below 5.0 m-bgs, with peak concentrations of TCE at the bottom of the core (2.8 mg/kg, 7.3 m-bgs), and peak concentrations of DCE near the same depth (i.e., 0.6 mg/kg between 6.0 – 7.3 m-bgs). DCE concentrations trend with TCE over depth, with some fluctuations. For example, at 5.0 m-bgs the molar ratio of TCE:DCE is approximately 1.0, and then varies between 0.70 – 3.0 along the remaining depth of the core. Similar trends are observed in the remaining CG85 cores (Figure 5). The fluctuations in TCE concentration with depth are partially related to the lithology, specifically the presence of the three recovered paleochannel sand lenses in CG85-4C at 4.6 – 4.9 m-bgs,

5.9 – 6.3 m-bgs, and 6.7 – 7.3 m-bgs. The four peaks of TCE concentrations in CG85-4C were measured in silty clay samples directly adjacent, both above and below, the two deeper sand lenses. The peaks of TCE concentrations in the remaining cores similarly occur in regions that correspond to the two lower sand lenses in CG85-4C, despite the lower amounts or lack of sands recovered in these cores (Figure 5). For example, peak TCE concentrations are from 5.3-6.1 m-bgs in CG85-01, 5.3-6.3 m-bgs in CG85-05, 5.5-5.9 m-bgs in CG85-2C, 5.0-5.8 m-bgs in CG85-3C, and 5.3-5.8 m-bgs in CG85-06, suggesting a hydraulic connection between the cores near these depth intervals. Transport in sand intervals is likely dominated by advection, while that in the silty clay by much slower advective transport and/or diffusion. Hence, the TCE fluctuations indicate that the relative amounts of TCE to DCE being transported by advection from the upgradient source zone are different from those being transported over much longer time periods in the silty/clay, possibly due to changes in source zone concentrations over time or biotic reduction of TCE to DCE.

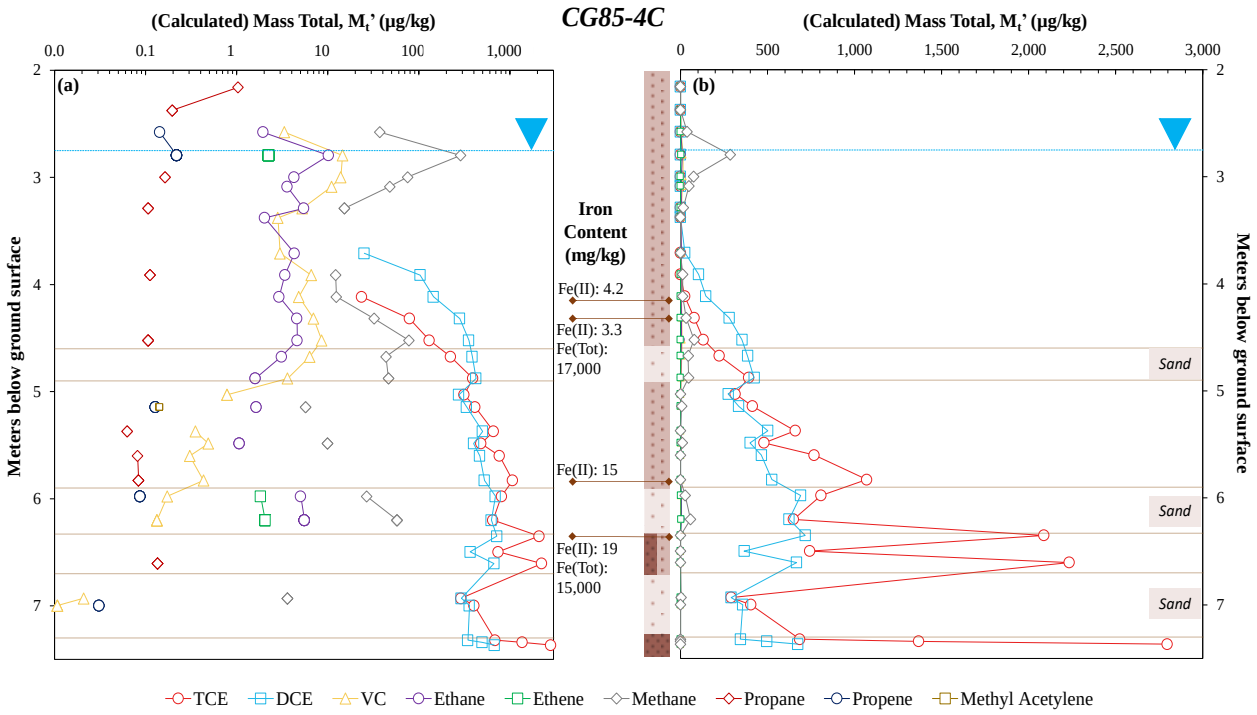

Figure 4: Concentration profiles for select VOCs from single core, CG85-4C, on two different axis scales. Samples from sand layers are normalized to mass of water (>95% of sample mass), not soil. Core lithology and results of iron analysis are also presented. Water table at 2.75 m-bgs, sand lenses are noted.

Again referring to CG85-4C, DCE concentrations only exceed TCE between 4.1 – 4.8 m-bgs, and above 4.1 m-bgs very little to no TCE and DCE is detected. Correspondingly, vinyl chloride (VC), ethane, and methane concentrations generally increase above 4.8 m-bgs. The same trends are observed in all other cores (Figure 5). Also, the concentration trends of VC, ethane, and methane follow one another closely through the shallow depth intervals (i.e., above 4.8 m-bgs) in all cores, albeit at different concentrations. Vinyl chloride is a well-established anaerobic biotic reduction product of TCE and DCE, and in prior reports VC was not identified in the DNAPL source zone (i.e., in MW-103) (Bloom et al., 2000). Transformation to VC is only possible when bacteria

from the *Dehalococcoides* genus are present (J. He et al., 2005), and it has been associated with strongly reducing methanogenic conditions (Duhamel & Edwards, 2007). Therefore, the presence of VC and methane, and the absence of TCE and DCE, are strong indicators that TCE and DCE were biologically reduced to VC in this region. The absence of measured ethene at most similar depth intervals makes it difficult to directly attribute ethane to biological VC reduction to ethene, but this appears to be the most likely pathway. Also, ethene could have been biotically or abiotically transformed to ethane, but it's not possible to distinguish these competing pathways from the measured profiles.

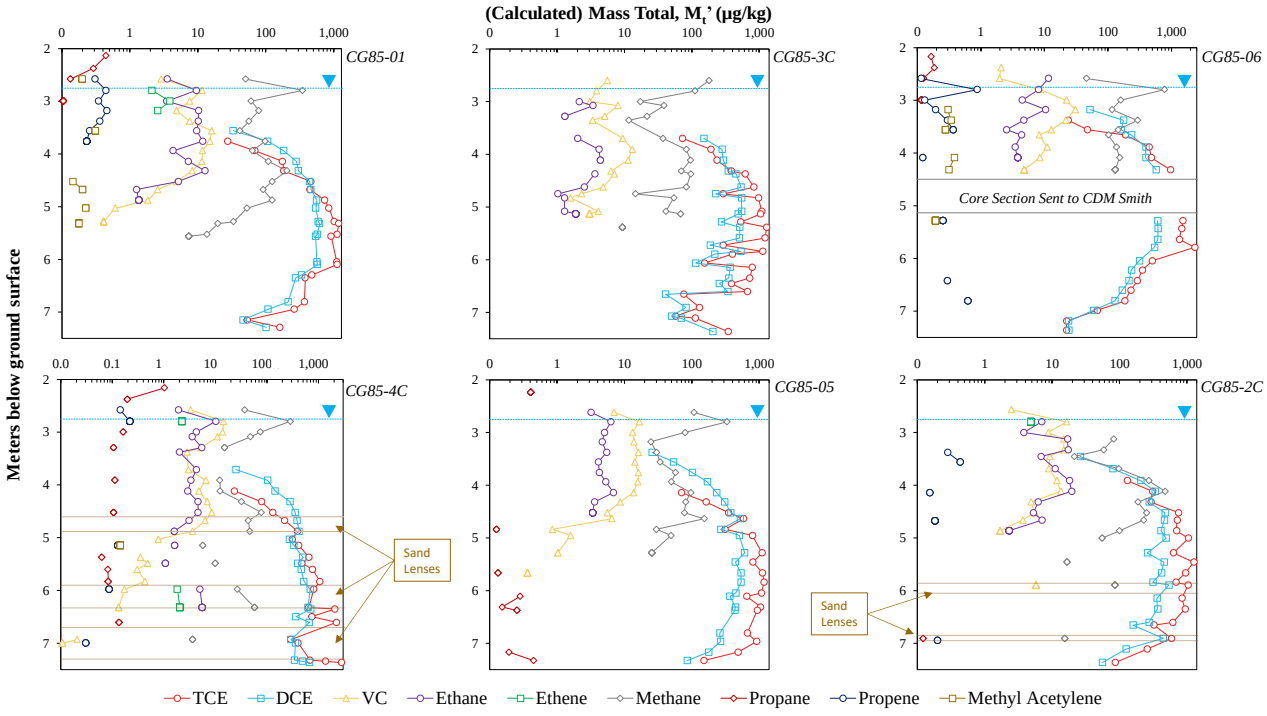

Figure 5: Concentration profiles for select VOCs for all six cores in CG85. Plot orientation is the same as orientation of the borings on-site. Water table at 2.75 m-bgs, all sand lenses are noted. Duplicate samples were taken for 10% of samples (duplicate = analysis of adjacent 'quarter' from 2.5 cm interval).

Biotic reduction of TCE to DCE and to VC requires an electron donor source, and one measure of this is the chemical oxygen demand (COD). Each mg/g of COD is equivalent to an electron donating capacity of 0.125 mmol-electrons/g, so this parameter was measured as a function of depth in two cores (i.e., CG85-4C, CG85-05) and results are presented in Figure S2. The COD concentrations trend slightly downward with increasing depth in CG85-4C and slightly upward with increasing depth in CG85-05. They vary from 0.4 to 3.0 mg-O2/g, corresponding to an electron donating capacity of 0.05 to 0.38 mmol-electrons/g. TCE and DCE concentrations are generally below 800 ug/kg, except for the 4 peaks adjacent to the two lower sand intervals that reach 2800 ug/kg. These concentrations correspond to an electron accepting capacity of 0.005 to 0.017 mmol-electrons/g for TCE transformation all the way to ethene. Hence, there appears to be sufficient electron donating capacity along the entire depth to sustain chloroethene reduction, suggesting that the more reducing conditions at shallower depths (i.e., above 4.8 ft-bgs) are promoting transformation to VC and possibly (via ethene) ethane.

While the evidence for biotic reduction of TCE and DCE to VC is strong, the evidence for abiotic reduction processes is not. Abiotic reductive processes are indicated by the presence of further reduced gas. Some of these were measured at the site, and these are propane and propene. However, their measured concentrations with depth are low and sporadic. For example, propane was measured at low but consistent concentrations at multiple depth intervals in CG85-4C (Figure 4), but at many other depth intervals it was not measured. Also, at the shallowest depth interval above the water table one relatively high concentration value was measured. Propene concentrations were similarly low, but in only a few measurement intervals at lower depths. In the remaining cores, propane and propene trends are generally similar, but propane and propene were detected in even fewer intervals. Also, the dominant abiotic transformation product observed in batch systems,

acetylene (Damgaard et al., 2013; Darlington et al., 2008), was not detected in any cores. A related product, methyl acetylene, was detected at a few depth intervals, but at low concentrations and not with any consistency. Abiotic reductive processes have been related to ferrous iron concentrations associated with sediments (Schaefer et al., 2018), and abiotic TCE reduction has appeared favorable at Fe(II) concentrations exceeding 100 mg/kg in batch experiments (Schaefer et al., 2021). Ferrous iron concentrations were measured at several depth intervals in CG85-4C, and values were always ≤19 mg Fe(II)/kg. Hence, the sporadic measurements of reduced gases, their lack of correlation to any CVOC concentrations, the absence of acetylene, and the low measured Fe(II) concentrations, all suggest that abiotic reduction processes are minimally impacting CVOC fate at the site. However, caution is advised with this interpretation, as reduced gas products are very susceptible to further biological degradation (Schloemer et al., 2016), and their absence provides only circumstantial evidence. Also, total iron concentrations are relatively high (15,000-17,000 mg Fe/kg), and it's possible that a larger reservoir of ferrous iron previously existed and was exhausted via biotic reduction of CVOC and possibly intruding oxygen.

3.3 VOC Recovery from Cryogenic Versus Conventional Cores Are Similar, With Limited Evidence of Better Recovery With Conventional Cores

To facilitate comparison of VOC recoveries between cryogenic and conventional cores, measurements from the same depth interval in cryogenic or conventional cores were combined as replicates, and then running averages were taken for cryogenic or conventional cores using three adjacent depth intervals (excluding values measured in sands). For either cryogenic or conventional cores, this resulted in nine measurements contributing to the average and standard deviation of each presented value. Results for

both headspace concentrations and total VOC masses, each per mass of dry soil, are shown in Figure 6 for TCE and DCE, and in Figure 7 for VC, methane, and ethane. Recall that headspace concentrations were directly measured, while total VOC masses were calculated from mass balance. The two profile types show only minor differences, and the latter (VOC mass profiles) are primarily affected by differences in vapor phase concentrations ($C_{g,i}$) between cryogenic and conventional samples, which when multiplied by $K_d/H_{cc,i}$ affect profile offsets.

TCE depth profiles of Cg' or Mt' for both cryogenic and conventional cores are very similar (Figure 6a,b), following the same trend with insignificant differences (i.e., overlapping values of standard deviation) between almost all 26 pairs of values. At only one depth for Mt', 5.4 m-bgs, did the conventional cores have a statistically significant higher (34%) value than the cryogenic cores. Interestingly, at intermediate depth intervals (5.0 – 6.0 m-bgs), the conventional cores consistently had 10-40% higher average Cg' and Mt' concentrations. This flips after 6.0 m-bgs, to the bottom of the cores (7.3 m-bgs), where the cryogenic cores then consistently had 50-100% higher average Cg' and Mt' concentrations. However, none of these differences are statistically significant per overlap of standard deviation values.

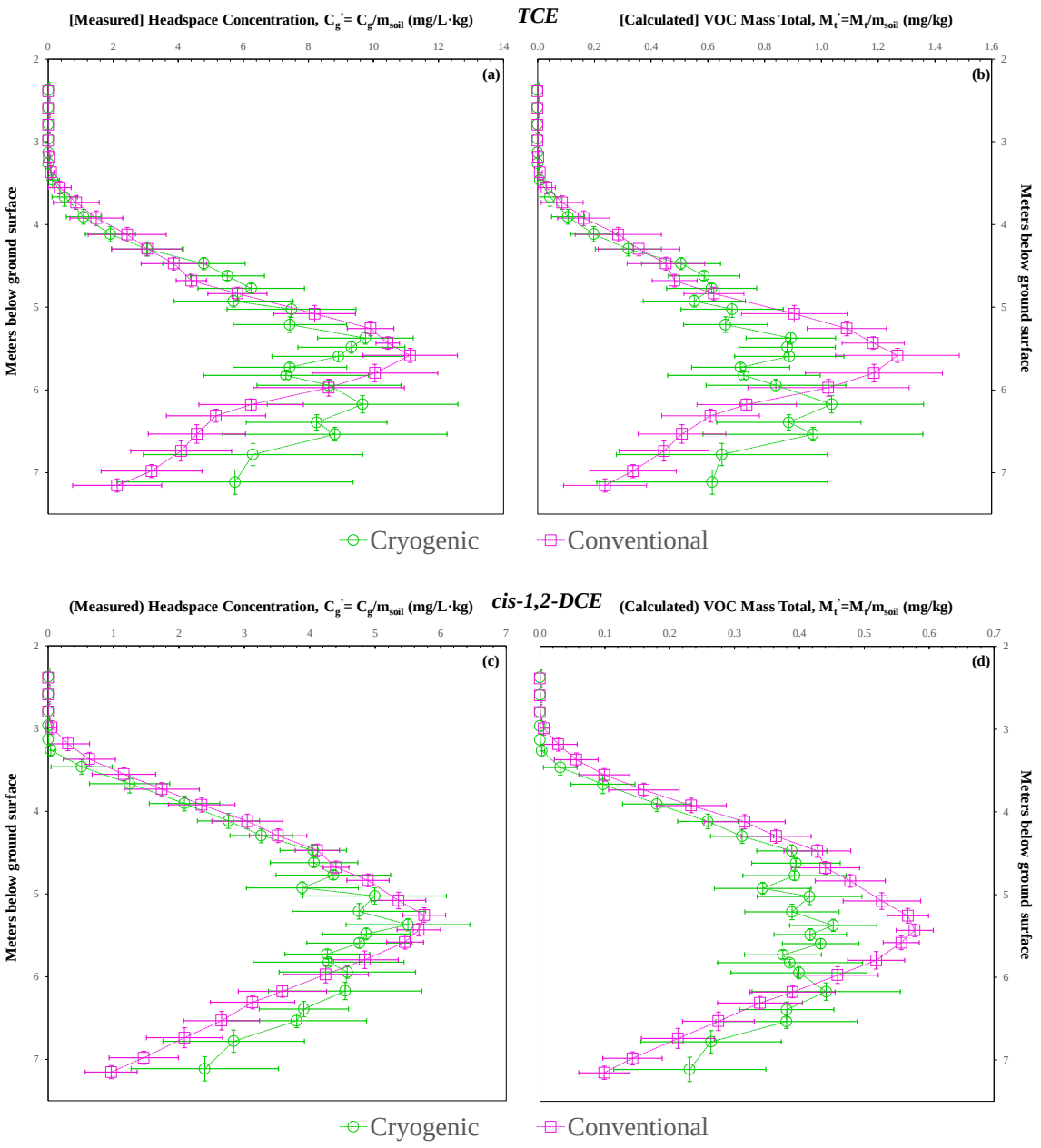

Figure 6: Running average TCE & DCE profiles for conventional and cryogenic core samples. Horizonal error bars are standard deviation of nine samples per point. Vertical error bars represent average of depths per points included.

DCE depth profile trends for cryogenic versus conventional cores are similar to those for TCE. Again, values of Mt' or Cg' for both cryogenic and conventional cores are similar at most depth intervals (Figure 6b,c), but there are more depth intervals (compared to TCE) where significant differences in Mt' occur. For example, Mt' values from conventional cores are significantly greater than those from cryogenic cores at three intermediate depth intervals between 5.2 – 5.6 m-bgs. Also, as with TCE, average DCE Cg' and Mt' concentrations from conventional cores are greater at intermediate depth intervals (5.0 – 6.0 m-bgs), while these concentrations from cryogenic cores are greater below 6.0 m-bgs. Again, however, none of these differences are statistically significant per overlap of standard deviation values.

As with TCE and DCE, the VC, ethane, or methane trends for cryogenic versus conventional cores are similar to each other, with slight differences across the intermediate depths (Figure 7). For example, with VC, the Mt' or Cg' values from conventional cores are significantly greater than those from cryogenic cores at three intermediate depth intervals (out of 19 total) between 3.4 – 3.8 m-bgs, where concentrations peak, and average values at these intervals differ by 50 to 135%. With ethane, the Mt' or Cg' values from the two coring methods are equivalent at all depths where ethane was present. Lastly, with methane, the Cg' values overlap, while Mt' values from conventional cores are significantly greater than those from cryogenic cores at two depth intervals (out of 20 total), just below where concentrations peak between 3.2 – 3.4 m-bgs. Average values at these intervals differ by approximately 225%. At all other depth intervals for methane, Mt' values between the two coring methods are not significantly different.

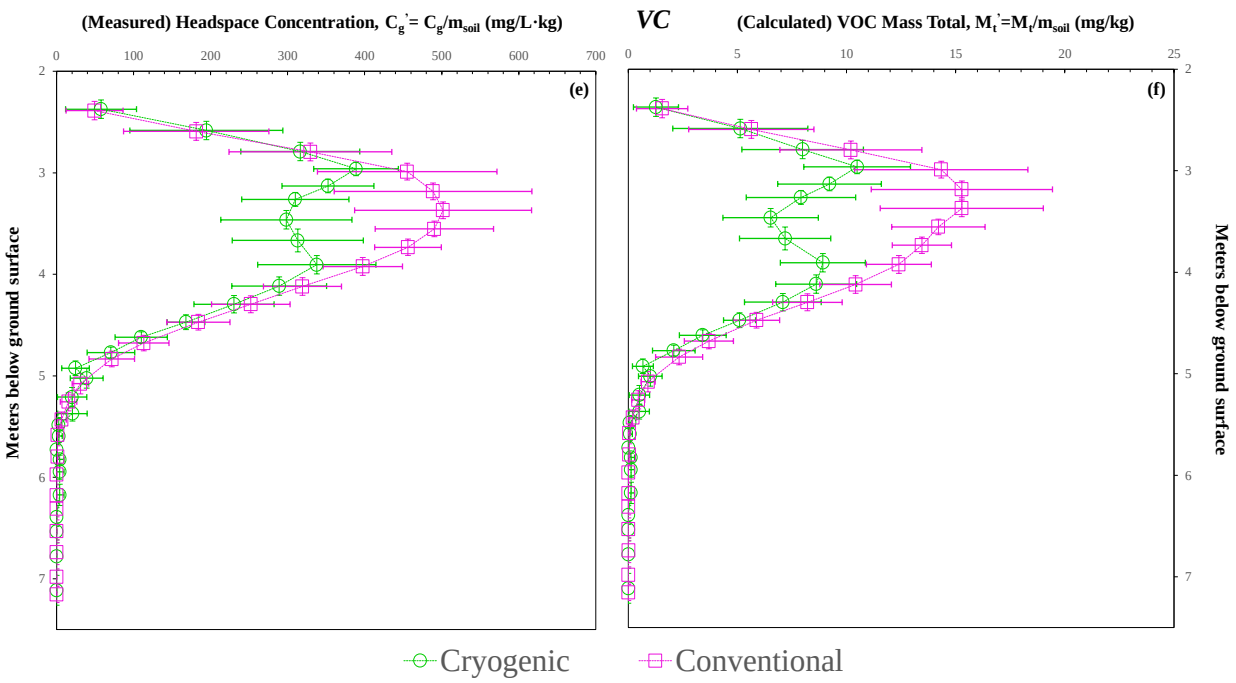
(Measured) Headspace Concentration, C_g'= C_g/m_{soil} (mg/L·kg)
VC
(Calculated) VOC Mass Total, M_t'=M_t/m_{soil} (mg/kg)
(e)
(f)
Meters below ground surface
Meters below ground surface
Cryogenic
Conventional

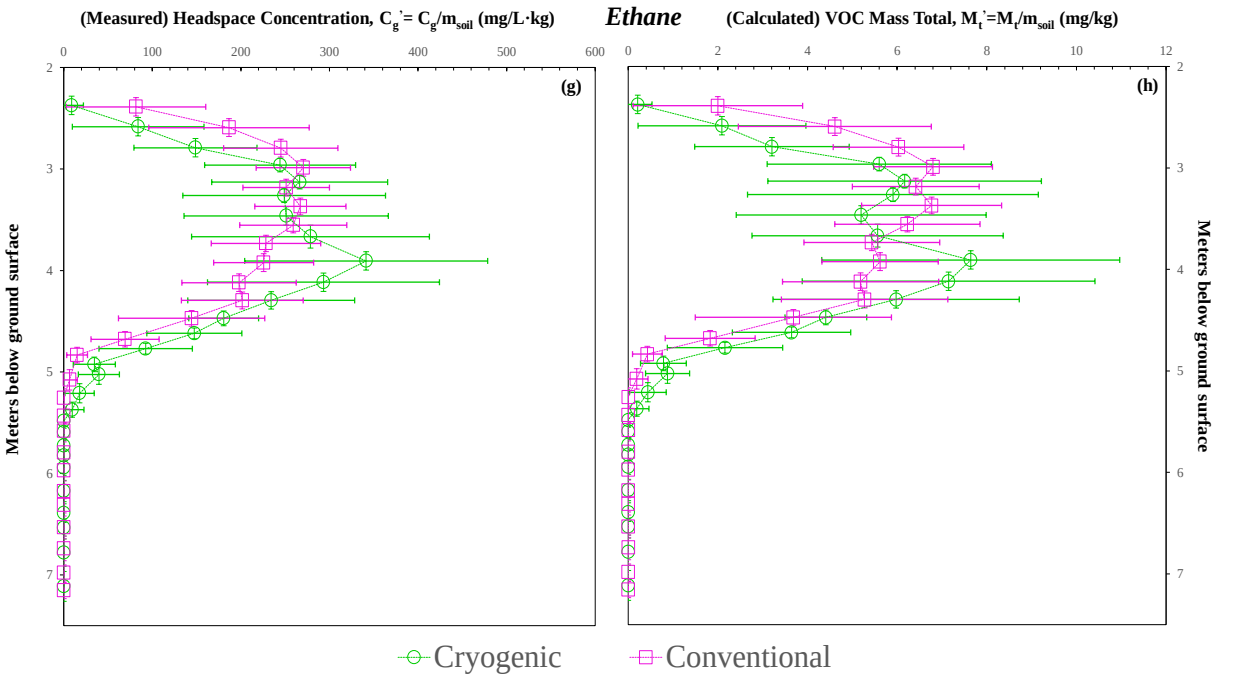
(Measured) Headspace Concentration, C_g'= C_g/m_{soil} (mg/L·kg)
Ethane
(Calculated) VOC Mass Total, M_t'=M_t/m_{soil} (mg/kg)
(g)
(h)
Meters below ground surface
Meters below ground surface
Cryogenic
Conventional

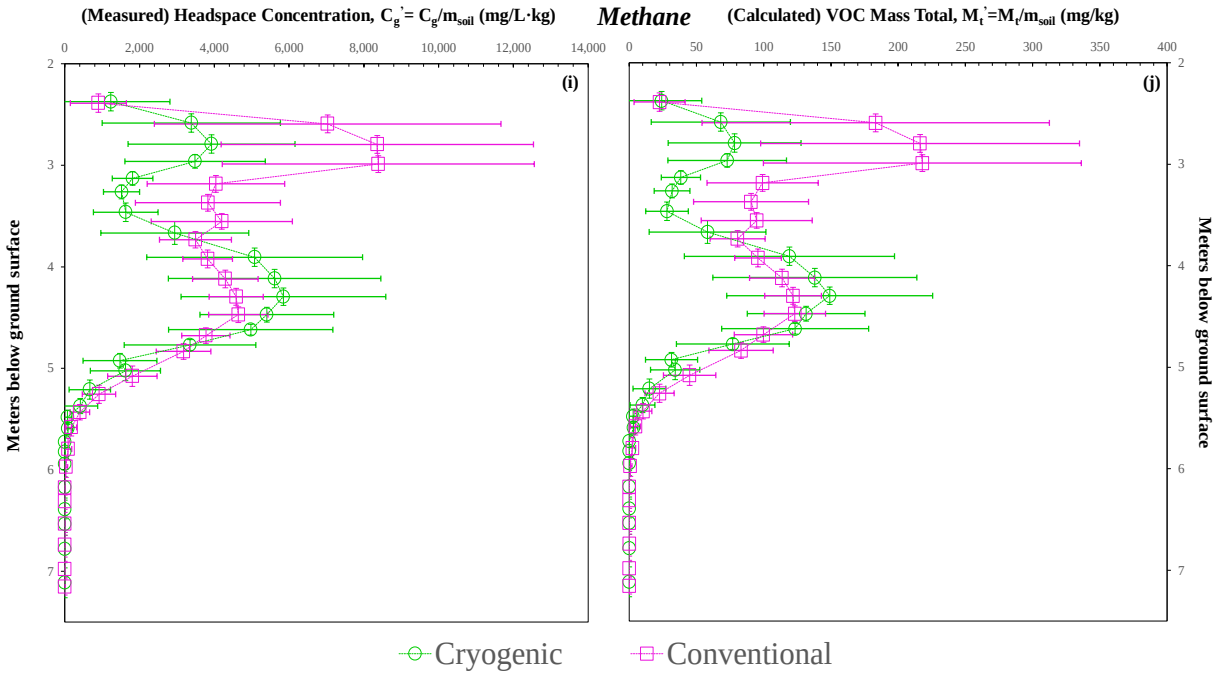

Figure 7: Running average VC, ethane, & methane profiles for conventional and cryogenic cores. Horizonal error bars are standard deviation of nine samples. Vertical error bars represent average of depths per points included.

Comparison of results for all five VOCs (Fig. 6-7) shows Cg' and Mt' concentrations are generally more variable for cryogenic versus conventional cores. This could be due to improved material recovery near sand lenses in cryogenic cores (Figure 3), allowing higher concentration peaks or lower concentration valleys to be captured at these depth intervals (e.g., Figures 4 and 5). As a result, there is more variability in Cg' and Mt' running averages.

Comparison of results for all five VOCs also shows that Cg' values among the two methods are generally indistinguishable, except at two depth intervals for VC where values from conventional cores exceed those from cryogenic cores. They show that values of Mt' are indistinguishable except near peak concentrations for four of five VOCs, where a

handful of values from conventional cores exceed those from cryogenic cores. Overall the results indicate that both cryogenic and conventional coring methods preserve CVOC and reduced gas concentrations in soil cores, with some evidence of slightly better preservation with conventional coring

There are several explanations to address the evidence supporting slightly better preservation of VOCs with conventional versus cryogenic coring. The first is insufficient sample numbers to adequately capture sample variability, such that with additional data the values of Cg' or Mt' from conventional and cryogenic cores would be indistinguishable at all depth intervals. This could be under sampling of frozen core intervals used to measure VOCs, or more likely error associated with the use of single input values for pore water saturation (θ_w), K_d, and ρ_b used in mass balance calculations to determine Mt'. These latter three values were determined from only several replicate values along the full length of the core and averaged due to their likeness. This could explain why there are more depth intervals with Mt' values from conventional cores exceeding those from cryogenic cores compared to Cg'.

Another possible explanation is that there is simply more VOC mass loss associated with cryogenic versus conventional coring methods, and the literature on water freezing may provide some insights. It is well established that lower freezing temperatures result in faster water freezing, and smaller ice crystal sizes (Kono et al., 2017; Mulot et al., 2019). Also, it's been shown that smaller ice crystals have lower melting temperatures (Chalmers, 1977; Martino & Zaritzky, 1987; Pan et al., 2011), and this is thought to result in faster melting compared to larger ice crystals (Tan et al., 2021). Cryogenic cores were frozen in-situ by circulating liquid nitrogen at -196°C around PVC sleeves containing soil. Conventional cores were brought to the surface at room temperature and placed in coolers with dry ice, at -78.5°C, and direct contact between soil cores and dry ice in coolers was

limited. Therefore, it is reasonable to assume that conventional cores froze more slowly than cryogenic cores, and ice crystal sizes in cryogenic cores are smaller than in conventional cores. All core sections were cut into 2.5 cm intervals that were crushed frozen and quickly funneled into glass serum bottles that were subsequently sealed. The energy from crushing (i.e., hammer impact) caused some ice melting, and it's possible that after crushing and before placement in sealed bottles more ice melted in samples from cryogenic than conventional cores and resulted in more VOC losses. While possible, insufficient sample numbers seem the more likely reason for differences in Cg' or Mt' between cryogenic and conventional cores.

4.0 Conclusion

- Cryogenic coring better preserves site lithology, recovering multiple, distinct paleochannel sand lenses that the adjacent conventional cores did not. Identification of these high permeability layers is key in understanding contaminant transport at a site.

- Deeper core depths are dominated by concentrations of TCE and DCE. The TCE to DCE ratios are similar to upgradient values, and attributed to diffusion into silty clay zones after advection from an upgradient source through the paleochannel sand lenses.

- Shallower core depths are dominated by concentrations of VC, ethane, and methane. The presence of methane suggests strongly reducing conditions resulted in biological reduction of TCE and DCE to VC. The similarity in VC and ethane concentration profiles suggests VC was further biologically reduced to ethene, which was either biotically or abiotically converted to ethane.

- Acetylene is the primary reduced gas product indicating abiotic TCE or DCE reduction, and it was not detected in any cores, although a possible reaction product methyl acetylene was detected. Other reduced gas products observed in lab experiments to result from this abiotic reaction pathway were observed, namely propane and propene. However, like methyl acetylene, their concentrations were very low and inconsistently detected relative to the aforementioned reaction products. Therefore, evidence of abiotic TCE and DCE reaction is not apparent.

- Running averages of headspace VOC concentrations and total VOC mass per mass of soil analyzed with depth were evaluated and compared for cryogenic versus conventional cores. TCE, DCE, VC, ethane, or methane profile shapes for cryogenic versus conventional cores were similar, showing minimum and maximum values at similar depths and typically with 50% of each other. However, marginally but significantly higher concentrations were obtained for some analytes from conventional core materials at peak concentration values, and concentration differences appeared greater for more volatile analytes (i.e.., VC, ethane, methane). This suggests that greater recovery of VOCs is possible with conventional compared to cryogenic coring, but this could be due to statistical under sampling and more studies are needed to support this data set.

This page is intentionally left blank.

Supporting Information

Measured Soil Recovery in Sample Core Liners

Table S1: Measured Recovery of Soil in Field for CG85 Cores

Depth	1		2C		3C		4C		5		6	
	Inches	**Feet**	**Inches**	**Feet**	**Inches**	**Feet**	**Inches**	**Feet**	**Inches**	**Feet**	**Inches**	**Feet**
7-9.5	33	2.75	34	2.83	31.5	2.63	33	2.75	31	2.58	32.5	2.71
9.5-12	30	2.50	26	2.17	22	1.83	23	1.92	29.5	2.46	29	2.42
12-14.5	30	2.50	33	2.75	32.5	2.71	32	2.67	31	2.58	34	2.83
14.5-17	28	2.33	27	2.25	36.5	3.04	28	2.33	25	2.08	23	1.92
17-19.5	19	1.58	31	2.58	36.5	3.04	37	3.08	31	2.58	28	2.33
19.5-22	20	1.67	36	3.00	36.5	3.04	37	3.08	21	1.75	30	2.50
22-24.5	27	2.25	36	3.00	35	2.92	37	3.08	28.5	2.38	30	2.50

*Recovery based on 2.5’ (30”) PVC liners. Recovery >30” represents slough on top of liner (e.g flowing sands or excess from previous) and was not included in this analysis.
*Intervals with loss of <5” shaded yellow and ≥5” shaded red.

Calculating Mass Total (M_t) from Cg

$$M_{tot} = M_{adsorbed} + M_{vapor} + M_{aqueous} = C_w K_d m_{soil} + C_g V_g + C_w V_w$$
$$M_{tot} = \frac{C_g}{H_{cc}} K_D m_{soil} + C_g V_g + \frac{C_g}{H_{cc}} V_w$$

Conversion equations,

$$K_D = K_{oc} f_{oc}$$
$$\log(K_{oc}) = \log(K_{ow}) - 0.21$$
$$H_{cc} = \frac{C_g}{C_w}$$

Constants

Table S2: CVOC Constants

Compound	**MW**	**H []**	**Log(Kow)**	**Koc**	**Kd**
TCE	131.4	0.421	2.42	162.181	1.508283
cis-1,2-DCE	96.95	0.167	1.86	44.66836	0.415416
Vinyl Chloride	62.5	1.108	1.46	17.78279	0.16538
Methane	16.04	26.914			Assume 0
Ethane	30.07	20.451			Assume 0
Ethene	28.05	9.326	1.13	8.317638	0.077354
Acetylene	26.04	0.888	0.37	1.44544	0.013443
Propane	44.1	28.918	2.36	141.2538	1.31366
Propylene	42.08	8.017	1.77	36.30781	0.337663
Propyne	40.06	0.45	0.94	5.370318	0.049944

Source: PubChem

Table S3: Soil Constants

Avg. Soil Fraction of Organic Content (f_{oc})	0.0093 (measured/calculated)
Porosity (n)	0.3 (assumed, clay/silty clay)
Avg. Bulk Density (ρ_B)	1.84 (measured/calculated)
Avg. Soil Water Content (%)	8.4% (measured/calculated)

GC-FID Standard Curve (examples)

*Note: Approximately 15 5-pt standard sets were created over the course of this experiment. Results only show the most recent standard used. Additionally, single mid-point standards were checked before each day of analysis and were always within 10% of expected peak area.

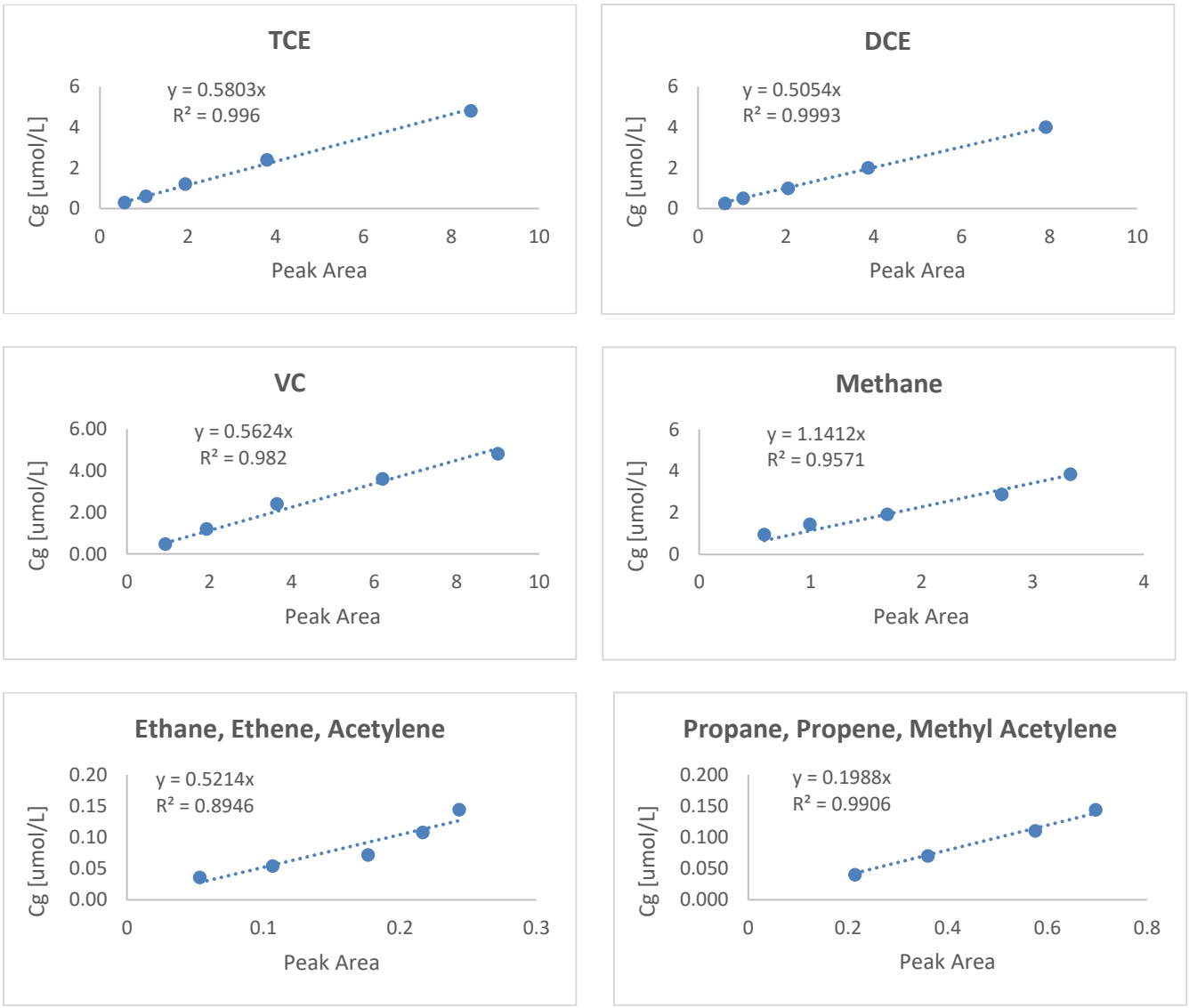

Figure S1: Sample of 5-pt standard plots used for GC-FID. Ethane/Ethene/Acetylene & Propane/Propene/Methyl Acetylene were averaged together due to likeness in peak area response.

COD Plots

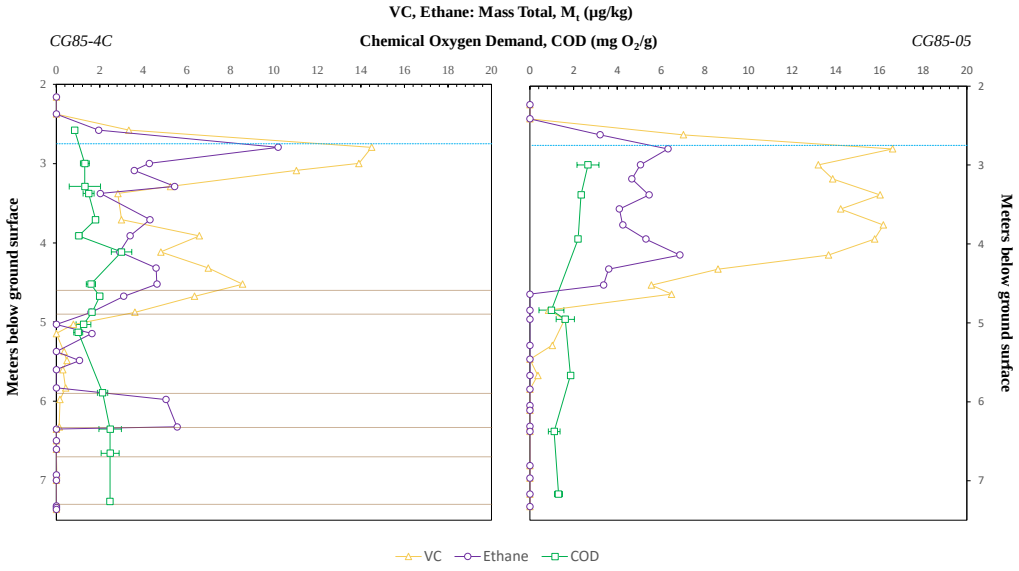

Figure S2: COD measurements with depth for CG85-4C and CG85-05.

References

Amonette, J. E., & Charles Templeton, J. (1998). Improvements to the quantitative assay of nonrefractory minerals for Fe(II) and total Fe using 1,10-phenanthroline. *Clays and Clay Minerals*, *46*(1), 51–62. https://doi.org/10.1346/CCMN.1998.0460106

Arnold, W. A., & Roberts, A. L. (2000). Pathways and kinetics of chlorinated ethylene and chlorinated acetylene reaction with Fe(0) particles. *Environmental Science and Technology*, *34*(9), 1794–1805. https://doi.org/10.1021/es990884q

Berns, E. C., Sanford, R. A., Valocchi, A. J., Strathmann, T. J., Schaefer, C. E., & Werth, C. J. (2019). Contributions of biotic and abiotic pathways to anaerobic trichloroethene transformation in low permeability source zones. *Journal of Contaminant Hydrology*, *224*, 1–25. https://doi.org/10.1016/j.jconhyd.2019.04.003

Bloom, Y., Aravena, R., Hunkeler, D., Edwards, E., & Frape, S. K. (2000). Carbon Isotope Fractionation during Microbial Dechlorination of Trichloroethene, *cis* -1,2-Dichloroethene, and Vinyl Chloride: Implications for Assessment of Natural Attenuation. *Environmental Science & Technology*, *34*(13), 2768–2772. https://doi.org/10.1021/es991179k

Butler, E. C., & Hayes, K. F. (2001). Factors influencing rates and products in the transformation of trichloroethylene by iron sulfide and iron metal. *Environmental Science and Technology*, *35*(19), 3884–3891. https://doi.org/10.1021/es010620f

C. Butler, E., & F. Hayes, K. (1999). Kinetics of the Transformation of Trichloroethylene and Tetrachloroethylene by Iron Sulfide. *Environmental Science & Technology*, *33*(12), 2021–2027. https://doi.org/10.1021/es9809455

Chalmers, B. (1977). *Principles of Solidification*. RE Krieger Pub.

Chapman, S. W., & Parker, B. L. (2005). Plume persistence due to aquitard back diffusion following dense nonaqueous phase liquid source removal or isolation. *Water Resources Research*, *41*(12), 1–16. https://doi.org/10.1029/2005WR004224

Culpepper, J. D., Scherer, M. M., Robinson, T. C., Neumann, A., Cwiertny, D., & Latta, D. E. (2018). Reduction of PCE and TCE by magnetite revisited. *Environmental Science: Processes and Impacts*, *20*(10), 1340–1349. https://doi.org/10.1039/c8em00286j

Damgaard, I., Bjerg, P. L., Bælum, J., Scheutz, C., Hunkeler, D., Jacobsen, C. S., Tuxen, N., & Broholm, M. M. (2013). Identification of chlorinated solvents degradation zones in clay till by high resolution chemical, microbial and compound specific isotope analysis. *Journal of Contaminant Hydrology*, *146*, 37–50. https://doi.org/10.1016/j.jconhyd.2012.11.010

Darlington, R., Lehmicke, L., Andrachek, R. G., & Freedman, D. L. (2008). Biotic and abiotic anaerobic transformations of trichloroethene and cis-1,2-dichloroethene in fractured sandstone. *Environmental Science and Technology*, *42*(12), 4323–4330. https://doi.org/10.1021/es702196a

Duhamel, M., & Edwards, E. A. (2007). Growth and Yields of Dechlorinators, Acetogens, and Methanogens during Reductive Dechlorination of Chlorinated

Ethenes and Dihaloelimination of 1,2-Dichloroethane. *Environmental Science & Technology*, *41*(7), 2303–2310. https://doi.org/10.1021/es062010r

Entwistle, J., Latta, D. E., Scherer, M. M., & Neumann, A. (2019). Abiotic Degradation of Chlorinated Solvents by Clay Minerals and Fe(II): Evidence for Reactive Mineral Intermediates. *Environmental Science and Technology*, *53*(24), 14308–14318. https://doi.org/10.1021/acs.est.9b04665

Environmental Protection Agency. (1998). *EPA Superfund Record of Decision: Lake City Army Ammunition Plant (NW Lagoon)*.

Ferrey, M. L., Wilkin, R. T., Ford, R. G., & Wilson, J. T. (2004). Nonbiological Removal of cis-Dichloroethylene and 1,1-Dichloroethylene in Aquifer Sediment Containing Magnetite. *Environmental Science and Technology*, *38*(6), 1746–1752. https://doi.org/10.1021/es0305609

Hayes, K. I. M. F. (1999). Trichloroethylene and Tetrachloroethylene by Iron Sulfide. *Environmental Science & Technology*, *33*(4), 2021–2027.

He, J., Sung, Y., Krajmalnik-Brown, R., Ritalahti, K. M., & Loffler, F. E. (2005). Isolation and characterization of Dehalococcoides sp. strain FL2, a trichloroethene (TCE)- and 1,2-dichloroethene-respiring anaerobe. *Environmental Microbiology*, *7*(9), 1442–1450. https://doi.org/10.1111/j.1462-2920.2005.00830.x

He, Y. T., Wilson, J. T., Su, C., & Wilkin, R. T. (2015). Review of Abiotic Degradation of Chlorinated Solvents by Reactive Iron Minerals in Aquifers. *Groundwater Monitoring and Remediation*, *35*(3), 57–75. https://doi.org/10.1111/gwmr.12111

He, Y. T., Wilson, J. T., & Wilkin, R. T. (2010). Impact of iron sulfide transformation on trichloroethylene degradation. *Geochimica et Cosmochimica Acta*, *74*(7), 2025–2039. https://doi.org/10.1016/j.gca.2010.01.013

Jeong, H. Y., & Hayes, K. F. (2007). Reductive dechlorination of tetrachloroethylene and trichloroethylene by mackinawite (FeS) in the presence of metals: Reaction rates. *Environmental Science and Technology*, *41*(18), 6390–6396. https://doi.org/10.1021/es0706394

KARICKHOFF, S., BROWN, D., & SCOTT, T. (1979). Sorption of hydrophobic pollutants on natural sediments. *Water Research*, *13*(3), 241–248. https://doi.org/10.1016/0043-1354(79)90201-X

Keller, K., Graff, T., & Buechler, T. (2003). *Lessons Learned from the Installation and Monitoring of a Permeable Reactive Barrier at the Lake City Army Ammunition Plant, Independence, MO*.

Kiaalhosseini, S., Johnson, R. L., Rogers, R. C., Renno, M. I., Lyverse, M., & Sale, T. C. (2016). Cryogenic Core Collection (C3) from Unconsolidated Subsurface Media. *Groundwater Monitoring and Remediation*, *36*(4), 41–49. https://doi.org/10.1111/gwmr.12186

Kocur, C. M. D., Fan, D., Tratnyek, P. G., & Johnson, R. L. (2020). Predicting Abiotic Reduction Rates Using Cryogenically Collected Soil Cores and Mediated Reduction Potential Measurements. *Environmental Science and Technology Letters*, *7*(1), 20–26. https://doi.org/10.1021/acs.estlett.9b00665

Koene-Cottaar, F. H. M., & Schraa, G. (2006). Anaerobic reduction of ethene to ethane in an enrichment culture. *FEMS Microbiology Ecology*, *25*(3), 251–256. https://doi.org/10.1111/j.1574-6941.1998.tb00477.x

Kono, S., Kon, M., Araki, T., & Sagara, Y. (2017). Effects of relationships among freezing rate, ice crystal size and color on surface color of frozen salmon fillet. *Journal of Food Engineering*, *214*, 158–165. https://doi.org/10.1016/j.jfoodeng.2017.06.023

Lee, W., & Batchelor, B. (2002). Abiotic reductive dechlorination of chlorinated ethylenes by iron-bearing soil minerals. 1. Pyrite and magnetite. *Environmental Science and Technology*, *36*(23), 5147–5154. https://doi.org/10.1021/es025836b

Lee, W., & Batchelor, B. (2004). Abiotic reductive dechlorination of chlorinated ethylenes by iron-bearing phyllosilicates. *Chemosphere*, *56*(10), 999–1009. https://doi.org/10.1016/j.chemosphere.2004.05.015

Martino, M., & Zaritzky, N. (1987). Effects of temperature on recrystallization in polycrystalline ice. *Sciences Des Aliments*, *7*(1), 147–166.

McCall, W., Christy, T. M., Pipp, D., Terkelsen, M., Christensen, A., Weber, K., & Engelsen, P. (2014). Field Application of the Combined Membrane-Interface Probe and Hydraulic Profiling Tool (MiHpt). *Groundwater Monitoring & Remediation*, *34*(2), 85–95. https://doi.org/10.1111/gwmr.12051

Mulot, V., Fatou-Toutie, N., Benkhelifa, H., Pathier, D., & Flick, D. (2019). Investigating the effect of freezing operating conditions on microstructure of frozen minced beef using an innovative X-ray micro-computed tomography method. *Journal of Food Engineering*, *262*, 13–21. https://doi.org/10.1016/j.jfoodeng.2019.05.014

Pan, D., Liu, L.-M., Slater, B., Michaelides, A., & Wang, E. (2011). Melting the Ice: On the Relation between Melting Temperature and Size for Nanoscale Ice Crystals. *ACS Nano*, *5*(6), 4562–4569. https://doi.org/10.1021/nn200252w

Parker, B. L., Chapman, S. W., & Guilbeault, M. A. (2008). Plume persistence caused by back diffusion from thin clay layers in a sand aquifer following TCE source-zone hydraulic isolation. *Journal of Contaminant Hydrology*, *102*(1–2), 86–104. https://doi.org/10.1016/J.JCONHYD.2008.07.003

Richards, P. M., Liang, Y., Johnson, R. L., & Mattes, T. E. (2019). Cryogenic soil coring reveals coexistence of aerobic and anaerobic vinyl chloride degrading bacteria in a chlorinated ethene contaminated aquifer. *Water Research*, *157*, 281–291. https://doi.org/10.1016/J.WATRES.2019.03.059

Schaefer, C. E., Ho, P., Berns, E., & Werth, C. (2018). Mechanisms for Abiotic Dechlorination of Trichloroethene by Ferrous Minerals under Oxic and Anoxic Conditions in Natural Sediments. *Environmental Science and Technology*, *52*(23), 13747–13755. https://doi.org/10.1021/acs.est.8b04108

Schaefer, C. E., Ho, P., Berns, E., & Werth, C. (2021). Abiotic dechlorination in the presence of ferrous minerals. *Journal of Contaminant Hydrology*, *241*. https://doi.org/10.1016/j.jconhyd.2021.103839

Schaefer, C. E., Ho, P., Gurr, C., Berns, E., & Werth, C. (2017a). Abiotic dechlorination of chlorinated ethenes in natural clayey soils: Impacts of mineralogy and

temperature. *Journal of Contaminant Hydrology*, *206*(September), 10–17. https://doi.org/10.1016/j.jconhyd.2017.09.007

Schaefer, C. E., Ho, P., Gurr, C., Berns, E., & Werth, C. (2017b). Abiotic dechlorination of chlorinated ethenes in natural clayey soils: Impacts of mineralogy and temperature. *Journal of Contaminant Hydrology*, *206*(August), 10–17. https://doi.org/10.1016/j.jconhyd.2017.09.007

Schaefer, C. E., Towne, R. M., Lippincott, D. R., Lazouskaya, V., Fischer, T. B., Bishop, M. E., & Dong, H. (2013). Coupled Diffusion and Abiotic Reaction of Trichlorethene in Minimally Disturbed Rock Matrices. *Environmental Science & Technology*, *47*(9), 4291–4298. https://doi.org/10.1021/es400457s

Schloemer, S., Elbracht, J., Blumenberg, M., & Illing, C. J. (2016). Distribution and origin of dissolved methane, ethane and propane in shallow groundwater of Lower Saxony, Germany. *Applied Geochemistry*, *67*, 118–132. https://doi.org/10.1016/j.apgeochem.2016.02.005

Tan, M., Mei, J., & Xie, J. (2021). The Formation and Control of Ice Crystal and Its Impact on the Quality of Frozen Aquatic Products: A Review. *Crystals*, *11*(1), 68. https://doi.org/10.3390/cryst11010068

Vogel, T. M., & McCarty, P. L. (1985). Biotransformation of tetrachloroethylene to trichloroethylene, dichloroethylene, vinyl chloride, and carbon dioxide under methanogenic conditions. *Applied and Environmental Microbiology*, *49*(5), 1080–1083. https://doi.org/10.1128/aem.49.5.1080-1083.1985